JOURNAL OF MATERIALS SCIENCE 30 (1995) 860–868

Tensile mechanical behaviour of quenched and annealed isotactic polypropylene films over a wide range of strain rates
Part II *Relationship with microstructure*

N. ALBEROLA, M. FUGIER
Laboratoire Matériaux Composites, E.S.I.G.E.C., Université de Savoie, B.P. 1104, 73376 Le Bourget du Lac, France

D. PETIT, B. FILLON
Péchiney Centre de Recherches de Voreppe, Z.I. Centr' Alp, B.P. 27, 38340 Voreppe, France

The tensile mechanical behaviour of quenched and annealed isotactic polypropylene (iPP) films has been analysed over a wide range of strain rates, i.e. from 10^{-3} to $3\times10^{+2}\,s^{-1}$. Evolution of mechanical properties of such films versus strain rate has been analysed through the microstructure. Thus, both the Young's modulus and the yield stress could be mainly controlled not only by the crystallinity ratio but also by the physical cross-linking degree of the amorphous phase induced by crystalline entities. For a given crystallinity ratio, the drawability of quenched and annealed iPP films is mainly controlled by the sum of the effects induced by both the physical cross-linking degree of the amorphous phase and the perfection degree of the crystalline phase. The increase in annealing temperature leads to the opposite evolution of these two microstructural parameters and then to opposite effects on the drawability of films. Changes in original microstructure of quenched films induced by drawing at various draw ratios and at various strain rates are also discussed.

1. Introduction

There are many reports in the literature of work concerning the influence of the microstructure of semicrystalline polymers on the mechanical properties, i.e. the elastic behaviour, the ability of plastic deformation and fracture toughness. Thus, studies of mechanical behaviour of such polymers focus on the effects of various physical or chemical agents which can change the original microstructure, such as thermal history imparted during processing [1–6], subsequent annealings [6–10], physical ageing [11–13] and solvent treatments [14, 15] and radiation exposures [16].

It has been shown that tensile behaviour of semicrystalline polymers could be governed by the molecular weight [4, 5, 17, 18]. It was found that the plastic deformation ability of polymers depends not only on initial morphology and molecular characteristics, but also on both the test temperature and strain rate [4, 17–23].

Thus, the drawability of semicrystalline polymer increases with increasing experimental temperature. But such experiments must be considered with caution, because microstructure could change with test duration. Thus, for test temperatures above or below the glass transition, T_g, crystallization (and/or annealing treatments) or physical ageing could occur, respectively. On increasing the strain rate from $0.008\,s^{-1}$ to $8.3\,s^{-1}$, Rolando *et al.* [4] have shown that polypropylene films exhibit a drastic transition from ductile to brittle behaviour. Such a transition was also observed for other semicrystalline polymers [23] and also for amorphous polymers [24–26]. According to Rolando *et al.* [4], this dramatic transition could result from the decrease in the length of time necessary to adjust and absorb the applied load, on increasing the strain rate. Then, the two types of tensile behaviour could result from two types of mechanical relaxational processes. Thus, according to Roetling [22], the yield stress of amorphous polymers, over a wide range of strain rates and temperatures, can be described by the Ree–Eyring theory [27]. Then, at low strain rates, the yield point could be governed by the mechanical relaxation related to T_g and above a critical strain rate, the yield stress could depend on the mechanical subglass transition. Based on such an analysis, Roetling [20] describes the yield stress behaviour of isotactic polypropylene as the sum of the stresses due to two rate processes, i.e. the transition related to the glass transition and a process associated with the crystalline-phase melting temperature.

However, such a description of tensile behaviour of both amorphous and semicrystalline polymers has certain limits. For example, according to the Roetling's model [20, 22], the activation energy of the main

0022–2461

transition is considered to be constant whatever the temperature. But, it is well-known that this apparent energy is a function of temperature, in agreement with the WLF equation [28]. Moreover, in the description of the mechanical behaviour of semicrystalline polymers, the second process related to the melting of the crystalline phase invoked by Roetling [22] cannot be considered as a relaxation, because it is well known that melting is a first-order transition which is not frequency dependent.

According to Jang *et al.* [29], the existence of the two types of mechanical behaviour exhibited by isotactic polypropylene could result from the two kinds of deformation mode. At high deformation rates or at low temperatures, crazing in the crystalline phase is favoured, while, at low rates or high temperatures, shear yielding predominates. This agrees with Olf and Peterlin's conclusion [30].

At low strain rate, on increasing the deformation ratio, De Candia *et al.* [6] have shown that the initial spherulitic morphology is destroyed for draw ratio above the yield point, because of the drastic reduction of the local section and consequently high stress concentration. In agreement with Peterlin [31, 32], they propose that each spherulite could generate bundles of microfibrilles. Thus, according to Peterlin [31, 32], with increasing draw ratio, the Young's modulus and stress at break both change with the number of tie molecules.

Moreover, some crystallographic phase transformation could occur under high deformation as shown for polyethylene [33] and isotactic polypropylene [34, 35]. Thus, according to Saraf and Porter [35], a uniaxial compression test performed on isotactic polypropylene at a draw ratio above 16 could induce an order–disorder transition in the crystals with formation of a disordered phase, so-called the "smectic" phase. Such a phase was found to improve the drawability of the polymer.

Heat generation during drawing could also occur [36–38]. Thus, according to Peterlin [38], the deformational work in the neck of ductile materials could be converted to heat and then the local temperature of the sample increases in the neck. Consequently, the drawing of ductile materials occurs at a higher temperature than that of the environment, which is the drawing temperature. The extreme case, with no heat conduction to the environment, could occur at very fast drawing (adiabatic drawing).

Based on the microstructure analysis reported in Part I [39] of this paper, the aim of this work was to obtain evidence for the main microstructural parameters which govern the elastic behaviour and the drawability of quenched and annealed isotactic polypropylene (iPP) films over a wide strain-rate range, i.e. from 10^{-3} to $3 \times 10^{+2}\,s^{-1}$.

2. Experimental procedure

2.1. Materials

Sheets of quenched isotactic polypropylene films with thickness of about 100 μm were provided by CRV Pechiney. The average molecular weight and polydispersity index are, respectively, $\bar{M}_w = 250\,000$ and $I_p = 4$. Samples annealed for 10 min at 70 and 160 °C were also tested over a wide range of strain rates. The microstructure of quenched and annealed samples was discussed in Part I of this paper [39]. Tensile test measurements were carried out on dog-bone-shaped specimens (5 mm wide and 33 mm long in the gauge section).

2.2. Uniaxial tensile tests

2.2.1. Tensile tests at low strain rates

Uniaxial tensile tests were performed at room temperature in an Adamel Lhomargy testing machine equipped with a strain gauge extensometer. Ten replicates were run at each strain rate. The reported data are the average values. Measurements were made at various crosshead speeds ranging from 10–950 mm min^{-1}. Because the gauge length is 33 mm, these crosshead speeds imply strain rates from 0.005–0.5 s^{-1}. For each measurement, the load was increased just beyond the yield point which was taken as the peak of the load–elongation curve.

The load–elongation curves were converted into engineering stress–strain plots by dividing the measured load on the sample by the initial cross-sectional area of the sample and the elongation by the original gauge length. The engineering yield stress and strain are defined as σ_{ey} and ε_{ey}. The yield point in the load–elongation curve may not be identical to the peak of the true stress–true strain curve. Thus, the true stress was determined as follows

$$\sigma_t = \frac{F(1 + \varepsilon_e)}{S_o} \tag{1}$$

where F is the load, ε_e the elongation per unit length, and S_o the original cross-sectional area. The true yield stress, σ_{ty}, was obtained through the Considere plot [40]. True yield strain ε_{ty}, was taken to be the value of ε_e at the true yield stress. For each engineering strain rate, the following parameters are determined: Young's modulus; engineering yield stress, σ_{ey}, and yield strain, ε_{ey}; true yield stress, σ_{ty}, and strain ε_{ty}; and draw ratio, λ. Young's modulus, E, was calculated from the initial slope of the stress–strain plot. The draw ratio is defined as

$$\lambda = 1 + \varepsilon_e \tag{2}$$

Among the analysed samples, only that annealed at 160 °C exhibits fracture over such a strain-rate range. Then, for this sample, two parameters were defined in addition, i.e. the stress and the strain at break. In the following discussion, such parameters are, respectively, called σ_R (σ_{eR} or σ_{tR}) and ε_R (ε_{eR} or ε_{tR}).

2.2.2. Tensile tests at high strain rates

Tensile experiments at high strain rates ranging from 10 to $3 \times 10^{+2}\,s^{-1}$ were performed at room temperature by means of a new tensile VHS 25 servohydraulic machine provided by Schenk Company. The sample was gripped to a piston rod which is displaced

at a velocity in the 0.1–20 m s^{-1} rate range. The position of the piston rod and then the displacement of the sample versus time can be assessed by both the usual transducer and an optical extensometer. The load was measured versus time by means of a piezoelectric crystal ring of 250 N in the fixture assembly and placed on the fixed end of the specimen. In order to avoid inertial effects of the fixture assembly, special grips for films were used. Measurements were carried out at various piston rod velocities from 0.3–10 m s^{-1}. As the initial length of specimen was 33 mm, the corresponding strain rates were in the 10 to $3 \times 10^{+2}$ s^{-1} range. Then, for each strain rate, such a setup provided the evolution of both load and specimen displacement versus time. Such curves were converted into usual engineering stress–strain plots according to the method described above. For each measurement, Young's modulus, E, stress at break, σ_R (σ_{eR} or σ_{tR}) and strain at break, ε_R (ε_{eR} or ε_{tR}), were determined. In addition, for the sample annealed at 70 °C, engineering and true yield stress and strain were evaluated.

2.3. Differential scanning calorimetry (DSC)

Changes in microstructure induced by drawing were investigated by means of DSC. Thus, for quenched iPP film, samples were cut from drawn dog-bone-shaped specimens in the centre between the grips where necking or failure occurs. At low strain, i.e. 0.05 s^{-1} (100 mm min^{-1}), the changes in microstructure in such a sample were analysed at various draw ratios, i.e. from 1–7.

2.4. Wide-angle X-ray diffraction (WAXD)

Samples cut from the neck region of quenched iPP films drawn at $\lambda = 7$ at various strain rates were also analysed by WAXD. Diffraction profiles were recorded by means of a Siemens D500 diffractometer using CuK_α between 5° and 50° with a 0.02° scan.

3. Results and discussion

3.1. Tensile mechanical behaviour

Fig. 1 shows the engineering and true stress–strain curves recorded for the quenched sample at low strain rate, i.e. 0.05 s^{-1}. It is noted that engineering and true yield stresses are almost equal. For such a strain rate, no fracture occurs and the sample displays a well-defined yield point followed by a steep drop in stress before necking occurs.

Hardening becomes noticeable at about 400% engineering strain. Quenched film can be extended to over 600%, at which point the machine extension limit is reached and sample fracture does not occur. Thus, quenched iPP drawn at 0.05 s^{-1} exhibits an engineering yield stress of about 21 MPa and a Young's modulus of 660 MPa.

Fig. 2 shows engineering stress–strain curves recorded at various strain rates from 0.05–200 s^{-1} for the quenched film. No fracture occurs in samples drawn at 0.05 and 0.5 s^{-1}. At higher strain rates, i.e. 10, 105 and 200 s^{-1}, samples become brittle. Thus, such a sample exhibits two kinds of mechanical behaviour, i.e. ductile then brittle, with increasing strain rate. Then, the drawability of quenched iPP films decreases with increasing deformation rate.

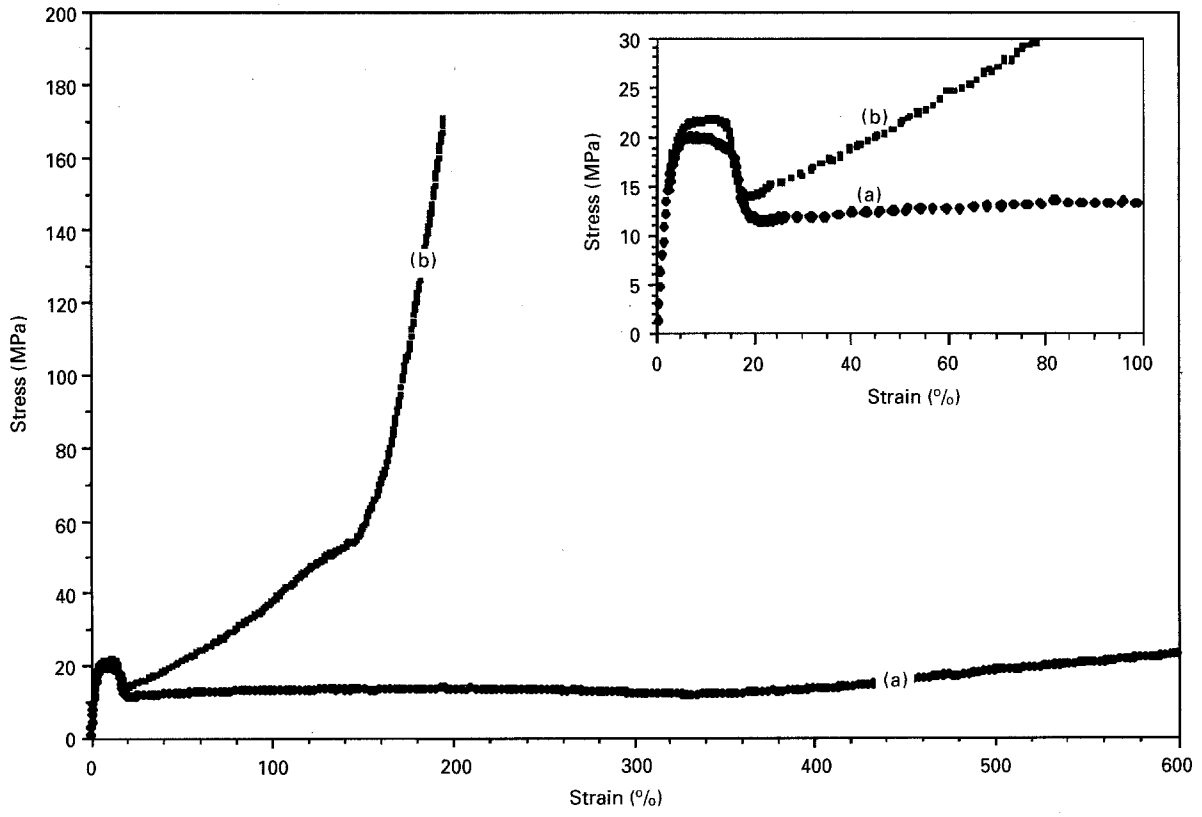

Figure 1 (a) Engineering and (b) true stress–strain curves of quenched iPP film drawn at 0.05 s^{-1}. Inset: an enlargement of the yield-point region.

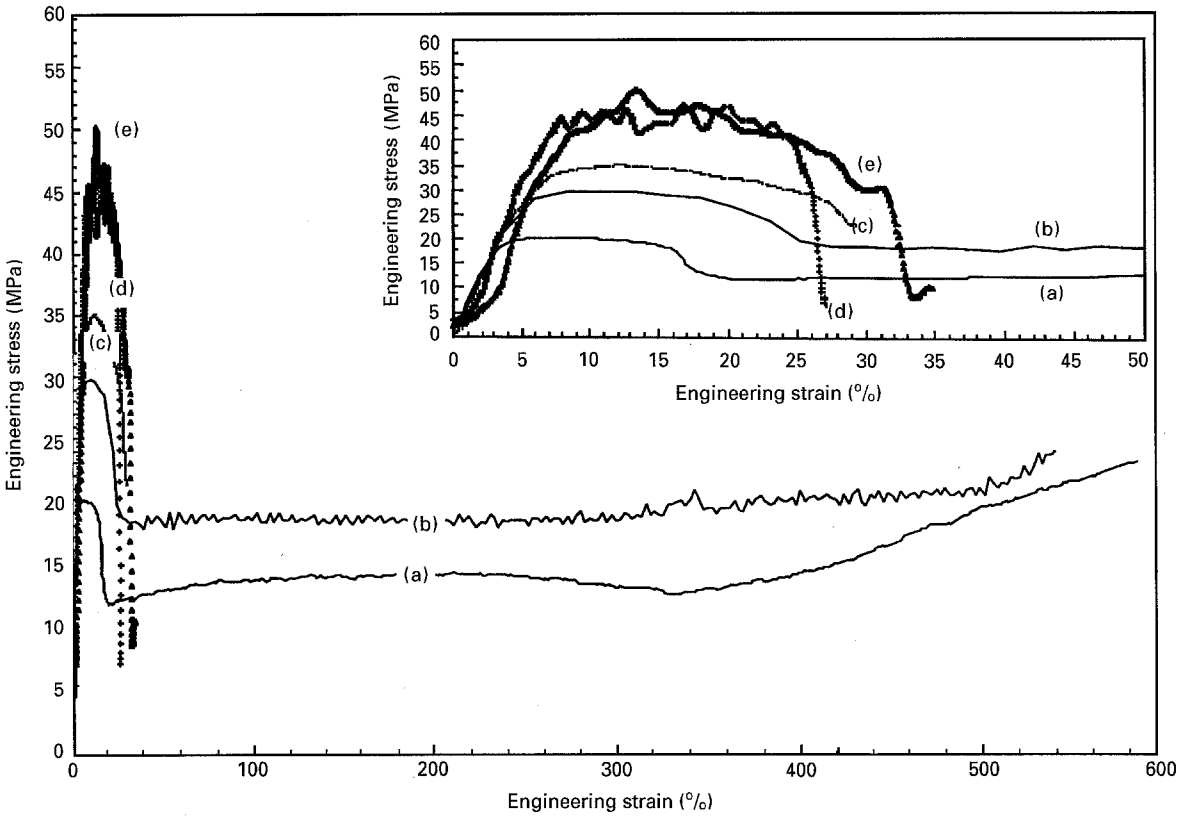

Figure 2 Engineering stress–strain curves of quenched iPP film drawn at (a) 0.05 s^{-1}, (b) 0.5 s^{-1}, (c) 10 s^{-1}, (d) 105 s^{-1} and (e) 200 s^{-1}. Inset: an enlargement of the yield-point region.

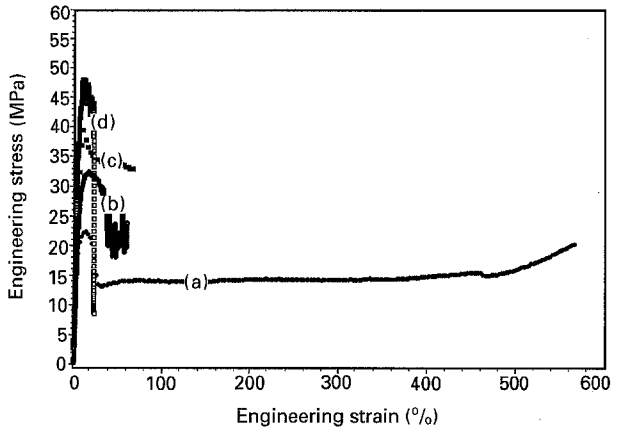

Figure 3 Engineering stress–strain curves of the samples annealed at (a, b) 70 °C and (c, d) 160 °C and drawn at (a, c) 0.5 s^{-1} and (b, d) 10 s^{-1}.

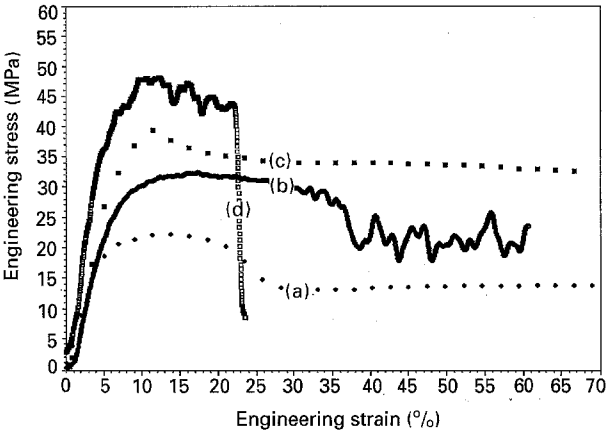

Figure 4 Enlargements of the yield-point region for the samples annealed at (a, b) 70 °C and (c, d) 160 °C and drawn at (a, c) 0.5 s^{-1} and (b, d) 10 s^{-1}.

As an example, Fig. 3 shows the engineering stress–strain curves recorded for the samples annealed at 70 °C and 160 °C at low and high strain rates, i.e. 0.5 and 10 s^{-1}. Fig. 4 shows, more precisely, the stress–strain curves recorded in the yield-point region. Only the sample annealed at 70 °C exhibits a well-defined yield point followed by a drop in stress. In contrast, at high strain rate, the sample annealed at 160 °C exhibits a rough brittle behaviour without neck forming.

Tables I and II report the engineering and true mechanical characteristics for the quenched film and the samples annealed at 70 and 160 °C drawn at 0.5 and at 10 s^{-1}.

3.1.1. Evolution of the Young's modulus and yield stress versus the strain rate

Figs 5 and 6, show the evolution of the Young's modulus and engineering yield stress, respectively, with the logarithm of the engineering strain rate for the quenched film and the annealed samples at 70 and 160 °C. Similar variation of the true yield stress versus strain rate is observed. For any thermal treatment, it can be observed that both the Young's modulus and the yield stress tend to increase with increasing strain rate. Only the sample annealed at 70 °C exhibits a yield point for strain rates above 1 s^{-1}. The quenched film and the sample annealed at 160 °C exhibits a brittle behaviour at high strain rates.

TABLE I Values of engineering and true mechanical characteristics for samples annealed at various temperatures and drawn at 0.5 s^{-1} at room temperature

Annealing temperature (°C)	Engineering				True				E (MPa)
	σ_{ey} (MPa)	ε_{ey} (%)	σ_{eR} (MPa)	ε_{eR} (%)	σ_{ty} (MPa)	ε_{ty} (%)	σ_{tR} (MPa)	ε_{tR} (%)	
20 (quenched)	28	9	–	–	31	9	–	–	630
70	21	14	–	–	25	13	–	–	440
160	40	11	38	67	44	11	64	52	740

TABLE II Values of engineering and true mechanical characteristics for samples annealed at various temperatures and drawn at 10 s^{-1} at room temperature

Annealing temperature (°C)	Engineering				True				E (MPa)
	σ_{ey} (MPa)	ε_{ey} (%)	σ_{eR} (MPa)	ε_{eR} (%)	σ_{ty} (MPa)	ε_{ty} (%)	σ_{tR} (MPa)	ε_{tR} (%)	
20 (quenched)	–	–	35	10	–	–	38	10	680
70	30	15	20	50	34	14	30	41	580
160	–	–	49	9	–	–	53	9	1100

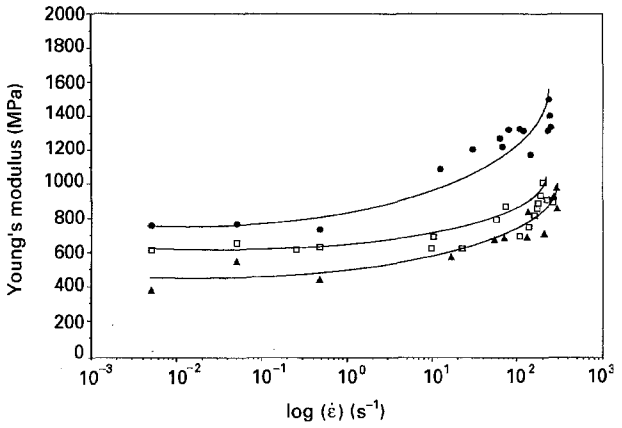

Figure 5 Evolution of the Young's modulus, E, with the logarithm of the engineering strain rate for (□) the quenched film and for the samples annealed at (▲) 70 °C and (●) 160 °C.

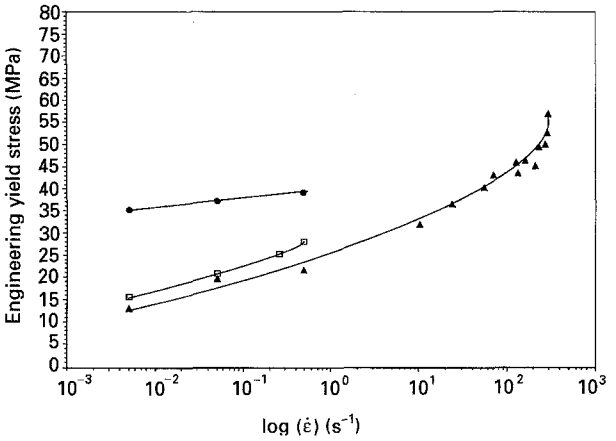

Figure 6 Evolution of the engineering yield stress versus the logarithm of the engineering strain rate for (□) the quenched film and for samples annealed at (▲) 70 °C and (●) 160 °C.

Moreover, for the sample annealed at 70 °C, a strong increase in the yield stress is observed for strain rates above 10 s^{-1}.

Such a strain-rate dependence of E and σ_{ey} is consistent with the relaxational character of the glass transition, which is located at about room temperature, i.e. at the tensile test temperature. Thus, with increasing the strain rate, the amorphous phase of the analysed samples progressively behaves as a glassy material, and both the apparent modulus and σ_{ey} increase.

Moreover, over the analysed strain-rate range, the sample annealed at 70 °C tends to exhibit the lowest value of Young's modulus, in particular, lower than that displayed by the quenched film, which shows the same crystallinity ratio. Thus, it can be proposed that the apparent modulus of iPP film is governed not only by the crystallinity ratio but also by the physical cross-linking degree of the amorphous phase induced by the crystalline phase. In fact, from microstructure analysis reported in Part I [39], it was shown that the annealing at 70 °C leads to an increase in the size of the crystalline entities and then to a decrease in the physical cross-linking degree of the amorphous phase. Furthermore, whatever the strain rate, the sample annealed at 160 °C displays the highest value of Young's modulus. It should be recalled that such a sample exhibits the highest crystallinity ratio. Thus, we can conclude that the strong reinforcement effect induced by the high crystallinity ratio is not counterbalanced by the weak physical cross-linking degree of the amorphous phase of such a sample, as determined in Part I.

3.1.2. Evolution of the stress and strain at break versus the strain rate

Figs 7 and 8 show the evolution of the engineering stress, σ_{eR}, and strain ε_{eR}, at break, respectively, versus the logarithm of the engineering strain rate for the quenched film and the samples annealed at 70 and 160 °C. Only the sample annealed at 160 °C exhibits

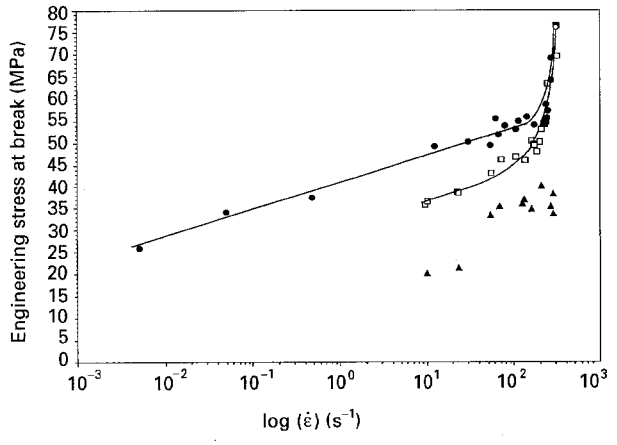

Figure 7 Variation of the engineering stress at break versus the logarithm of the engineering strain rate for (□) the quenched film and for samples annealed at (▲) 70 °C and (●) 160 °C.

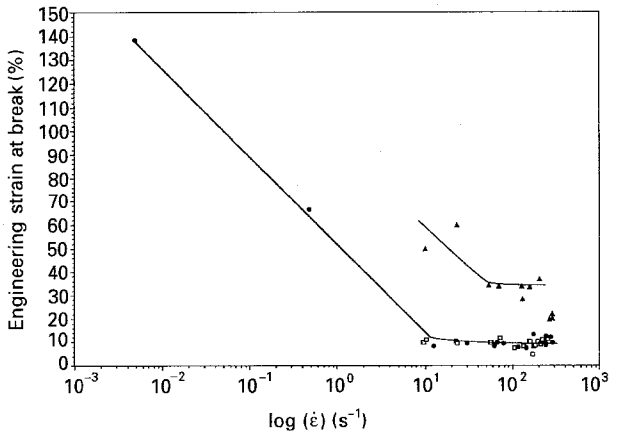

Figure 8 Evolution of the engineering strain at break versus the logarithm of the engineering strain rate for (□) the quenched film and for samples annealed at (▲) 70 °C and (●) 160 °C.

fracture at low strain rates, i.e. at strain rates less than $1\ s^{-1}$. In such a strain-rate range, the quenched film and the sample annealed at 70 °C both exhibit a ductile behaviour. For strain rates above $10\ s^{-1}$, the quenched film and the sample annealed at 160 °C exhibit a drastic increase in the stress at break. Moreover, on increasing the strain rate from $0.005\ s^{-1}$ to $1\ s^{-1}$, the strain at break of the sample annealed at 160 °C strongly decreases and then remains almost constant for strain rates above $10\ s^{-1}$. It is noted that the strain at break of the quenched film also remains constant for strain rates above $10\ s^{-1}$ and equal to that displayed by the sample annealed at 160 °C. In contrast, the strain at break of the sample annealed at 70 °C progressively decreases on increasing strain rate to above $10\ s^{-1}$, but it remains higher than the low value reached by both the quenched film and the annealed sample at 160 °C. Thus, the sample annealed at 70°C exhibits the highest drawability, in particular, greater than that displayed by the quenched iPP film which shows the same crystallinity ratio.

Previously, it was shown that the "elastic" properties, i.e. apparent modulus and yield stress, are mainly governed by both the crystallinity ratio and the molecular motion ability of the amorphous phase. To interpret the changes in drawability, we must consider, in addition, the perfection degree of the crystalline phase. In fact, assuming the iPP film to be composite materials constituted by an amorphous phase reinforced with a crystalline phase, it can be deduced that the deformation of the film results from the following macroscopic mechanisms. On drawing, whatever the rate of deformation, the amorphous phase first undergoes applied stress, because it is more disordered and softer than the crystalline phase. The deformation ability of the amorphous phase could depend on the molecular motion ability of the macromolecular chains of such a phase, i.e. the ability of chains in the amorphous phase to be extended along the draw direction. Then, the amorphous phase can impart stress to the crystalline entities whose plastic deformation ability is governed by the crystal defect concentration. Thus, the sample annealed at 70 °C exhibits the highest drawability, in particular, greater than that displayed by the quenched iPP film which has the same crystallinity ratio. It is proposed that for the annealing treatment at 70 °C, the sum of the effects on drawability induced by both the increase in degree of perfection of the crystalline phase and the decrease in physical cross-linking degree of the amorphous phase, could pass through an optimum. For the sample annealed at 70 °C, the lower drawability exhibited by the quenched iPP film could result from the strong physical cross-linking degree of the amorphous phase by many crystalline entities, in spite of the lowest degree of perfection of the microcrystallites exhibited by the as-received film. In contrast, the sample annealed at 160 °C exhibits the weakest drawability. The brittleness displayed by the sample annealed at 160 °C could mainly result from both the high crystallinity ratio and degree of perfection of crystallites. Such effects are not counterbalanced by the increase in molecular mobility of chains in the amorphous phase shown by such a sample.

The drastic change in the mechanical behaviour exhibited by the quenched film and the sample annealed at 160 °C, for strain rates above $10\ s^{-1}$, could correspond to a change in the mechanisms of fracture, i.e. at strain rates less than $10\ s^{-1}$, the amorphous phase of iPP samples rather behaves as a viscoelastic material and shear yielding could predominate, while at higher strain rates, the amorphous phase behaves as an elastic material (glassy material) and then brittle behaviour and crazing are favoured.

3.2. Changes in microstructure of quenched film after drawing

3.2.1. Microstructure evolution of samples drawn at low strain rates

Quenched iPP films drawn at low strain rates, i.e. from $0.005–0.5\ s^{-1}$, exhibit ductile behaviour. In order to obtain evidence for microstructure evolution occurring on drawing, samples were cut in the centre of the dog-bone-shaped specimens drawn at various λ values, i.e. from 1, corresponding to the yield point, to 7 related to the maximum of strain hardening.

For example, Fig. 9 shows the superimposition of the thermograms recorded at the same heating rate ($10\,°C\,min^{-1}$) for quenched iPP film undrawn and drawn at $\lambda = 4$ at $0.05\,s^{-1}$. Table III compares the values of the characteristic parameters determined from thermogram analysis for the samples drawn for various draw ratios at the same strain rate ($0.05\,s^{-1}$). The main changes in microstructure induced by drawing, on increasing the draw ratio, at low strain rates can be summarized as follows.

(i) At draw ratio $\lambda = 1$, which corresponds to the yield point, no change in original microstructure is detected.

(ii) At draw ratios above 1, the first endothermic peak (T_1), related to the melting of microcrystallites, is significantly shifted towards the lower temperature of about 20 °C, whatever the draw ratio. Thus, it can be concluded that original microcrystallites convert into crystalline entities exhibiting smaller size and/or a lower degree of perfection. It can be proposed that the addition of "crystallographic defects" induced by drawing in the original microcrystallites, which still exhibit a large disorder, could favour the progressive plastic deformation of such a paracrystalline phase. Then, in spite of an eventual increase in the local temperature in the neck region which could lead to annealing effects, i.e. an increase in both the size and the degree of perfection of crystallites, drawing, globally, could lead to a true chain unfolding of these distorted crystalline entities.

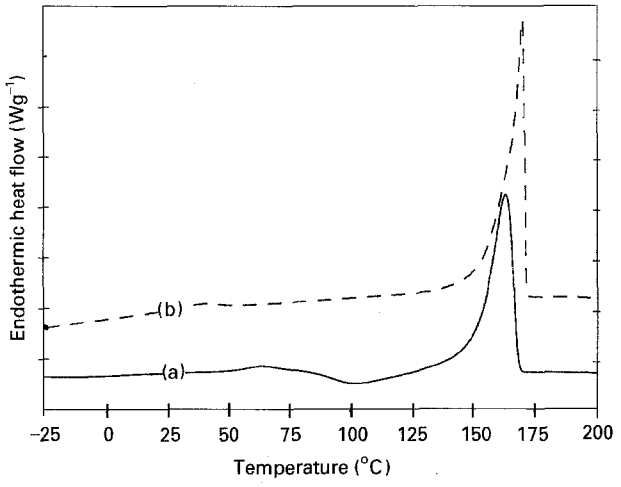

Figure 9 Thermograms recorded at $10\,°C\,min^{-1}$ for (a) the undrawn quenched iPP film and (b) a drawn ($\lambda = 4$) sample at an engineering strain rate of $0.05\,s^{-1}$.

TABLE III Characteristic parameters of thermograms recorded at $10\,°C\,min^{-1}$ for samples drawn at various draw ratios ($0.05\,s^{-1}$). T_1, temperature of the first endothermic peak; T_3, temperature of the upper endothermic peak; X_c, crystallinity ratio

Draw ratio, λ	T_1 (°C)	T_3 (°C)	X_c (%)
0	63	164	65
1	63	163	66
2	40	165	64
4	40	169	68
7	38	171	72

Consequently, the macromolecular chains in the amorphous phase can exhibit a better ability to extend along the draw direction, because of the decrease in the physical cross-linking degree of the amorphous phase.

(iii) For draw ratios above 2, the upper endothermic peak (T_3) related to the melting of the monoclinic phase is shifted towards the higher temperatures and the crystallinity ratio is increased. Thus, we suppose the formation of an additional more stable crystalline phase occurs, perhaps of monoclinic habit. But WAXD experiments do not provide evidence for such a formation of crystallites of monoclinic habit induced by drawing (see below). Thus, the shift of the T_3 peak towards the higher temperature could result from a better ability of the remaining crystalline entities to reorganize, on heating, into thicker and/or more perfect lamellae of monoclinic habit.

The WAXD spectrum recorded for a sample drawn at $\lambda = 7$ ($0.05\,s^{-1}$ strain rate) is shown in Fig. 10. Along and perpendicular to the drawing direction, there is a notable disappearance of the reflection profile located at about 21° (2θ). This suggests that the drawing could lead to a preferential orientation of the remaining crystallites along a direction intermediate between 0° and 90° with respect to the drawing direction.

Similar evolution of the original microstructure of quenched iPP film versus draw ratio was detected for samples drawn at other strain rates ranging from $0.005–0.5\,s^{-1}$.

3.2.2. Microstructural changes induced by drawing at high strain rates

Samples for analysis were cut in the broken region of specimens drawn at various high strain rates from $100–290\,s^{-1}$. Thermograms recorded at $50\,°C\,min^{-1}$ were compared to that displayed by the undrawn sample at the same heating rate. For example, Fig. 11 shows the superimposition of the thermograms recorded for the as-received film and the sample drawn at $170\,s^{-1}$. Table IV lists the characteristic parameter values determined from thermogram analysis (DSC)

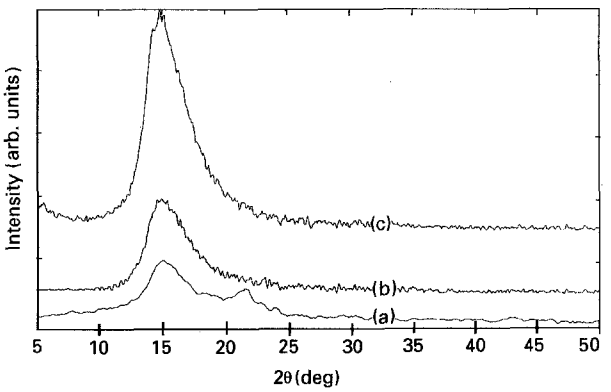

Figure 10 Wide-angle X-ray diffraction profiles of the quenched sample drawn at $\lambda = 7$ at an engineering strain rate of $0.05\,s^{-1}$ recorded (c) along and (b) perpendicular to the drawing direction. (a) Diffractogram of the undrawn sample is given as reference.

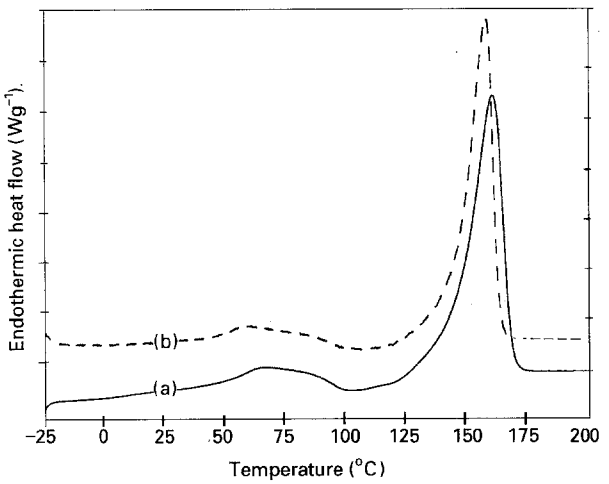

Figure 11 Thermograms recorded at 50 °C min^{-1} for (a) the undrawn quenched film and (b) for the broken sample tested at an engineering strain rate of 170 s^{-1}.

TABLE IV Characteristic parameters of thermograms recorded at 50 °C min^{-1} for samples drawn at various strain rates. T_1, temperature of the first endothermic peak; T_3, temperature of the upper endothermic peak; X_c, crystallinity ratio.

Engineering strain rate (s^{-1})	T_1 (°C)	T_3 (°C)	X_c (%)
0 (undrawn sample)	63	160	60
100	59	156	56
150	59	157	56
170	59	157	56
190	60	156	63
290	59	156	62

of samples drawn at the strain rates between 100 and 290 s^{-1}.

The main changes in the DSC characteristic values of broken samples with respect to those of the undrawn sample are:

(i) a constant shift of the T_1 and T_3 peaks towards the lower temperature of about 6 and 4 °C, respectively, whatever the strain rate;

(ii) no significant change in the crystallinity ratio. Thus, it can be concluded that drawing at high strain rate, globally, leads to a decrease in the size and/or the degree of perfection of the original microcrystallites. Such an effect appears to be less than that observed for samples drawn at lower strain rates. In fact, the shift of the T_1 peak towards lower temperatures (6 °C) is weaker than that observed for samples drawn at lower strain rates (20 °C). Thus, it can be proposed that, at high strain rates, the unfolding of the crystalline entities induced by drawing could be counterbalanced by annealing effects, because of an eventual increase in the local temperature. Moreover, with respect to the influence of drawing performed at low strain rate on the T_3 location, it can be noted that drawing at high strain rates acts in the opposite sense. The shift of the T_3 peak towards lower temperatures could show that crystallites of monoclinic habit, formed on heating from the melting of the microcrystallites, exhibit a smaller size and/or degree of perfection than those shown by undrawn samples. As no significant change in crystallinity ratio is detected, it can be concluded that drawing at such strain rates does not induce crystallization.

4. Conclusion

The tensile mechanical behaviour of quenched iPP film and samples annealed for 10 min at 70 and 160 °C was investigated at room temperature over a wide range of strain rates from 10^{-3} to $3\times10^{+2}$ s^{-1}. From analysis of the evolution of both yield stress and Young's modulus versus the annealing temperature, it is proposed that the elastic behaviour of quenched iPP films is mainly governed by the physical cross-linking degree of the amorphous phase and the crystallinity ratio.

The drawability of such samples is controlled not only by the microstructural parameters governing the elastic behaviour, but also by the degree of perfection of the crystalline entities.

Thus, on increasing the annealing temperature, the degree of perfection of the crystalline phase is increased, leading to a reduction in the plastic deformation ability of the crystalline phase while physical cross-linking degree of the amorphous phase is decreased. Thus, the sample annealed at 70 °C exhibits the greatest drawability because the sum of the opposite effects induced by such microstructural parameters passes through an optimum. The drawability of such films can also be influenced by the crystallinity ratio which acts in a similar way to the degree of perfection of the crystalline phase.

References

1. P. CEBE, S. Y. CHUNG and S. D. HONG, *J. Appl. Polym. Sci.* **33** (1987) 487.
2. A. A. OGALE and R. L. McCULLOUGH, *Compos. Sci. Technol.* **30** (1987) 185.
3. J. R. LLOYD, A. A. GOODWIN and J. N. HAY, *Br. Polym. Sci.* **23** (1990) 101.
4. R. J. ROLANDO, W. L. KRUEGER and H. W. MORRIS, *Plastics Rubber Proc. Appl.* **11** (1989) 135.
5. J. N. CHU, J. M. SCHULTZ, *J. Mater. Sci.* **24** (1989) 4538.
6. F. De CANDIA, R. RUSSO and V. VITTORIA, *J. Appl. Polym. Sci.* **34** (1987) 689.
7. P. Y. JAR and H. H. KAUSCH, *J. Polym. Sci. B Polym. Phys.* **30** (1992) 775.
8. A. ARZAK, J. Y. EGUIAZABAL and J. NAZABAL, *Polym. Eng. Sci.* **31** (1991) 586.
9. P. J. HENDRA, J. VILE, H. A. WILIS, V. ZICHY and M. E. A. CUDBY, *Polymer* **25** (1984) 785.
10. A. FICHERA and R. ZANNETTI. *Makromol. Chem.* **176** (1975) 1885.
11. J. N. HAY, D. J. KEMMISH, J. I. LANGFORD and A. I. M. RAE, *Polym. Commun.* **25** (1984) 175.
12. L. C. E. STRUIK, *Polymer* **28** (1987) 1521.
13. *Idem, ibid.* **28** (1987) 1534.
14. T. E. ATTWOOD, P. C. DAWSON, J. L. FREEMAN, L. R. J. HOY. J. B. ROSS and P. A. STANILAND, *ibid.* **22** (1981) 1096.
15. M. T. BISHOP, F. E. KARASZ, P. S. RUSSO and K. H. LANGLEY, *Macromolecules* **18** (1985) 86.
16. T. SASUGA and M. HAGIWARA, *Polymer* **26** (1985) 501.
17. N. BROWN and I. M. WARD, *J. Mater. Sci.* **18** (1983) 1405.
18. G. CAPPACIO and I. M. WARD, *Polymer* **15** (1974) 233.
19. R. J. ROLANDO, D. L. KRUEGER and H. W. MORRI, *Polym. Mater. Sci. Eng.* **52** (1985) 76.

20. J. A. ROETLING, *Polymer* **7** (1966) 303.
21. B. HARTMAN, G. F. LEE and W. WONG, *Polym. Eng. Sci.* **27** (1987) 823.
22. J. A. ROETLING, *Polym. Lond.* **6** (1965) 311.
23. P. BEGUELIN, M. BARBEZAT and H. H. KAUSCH, *J. Phys.* **(III) 1** (1991) 1867.
24. J. M. MURACCIOLE and Y. A. BERTIN, *ibid.* **(III) 1** (1991) 1881.
25. R. E. J. ROBERTSON, *J. Appl. Polym. Sci.* **7** (1963) 443.
26. S. WU, *Ibid.* **46** (1992) 619.
27. T. REE and H. EYRING, *J. Appl. Phys.* **26** (1955) 793.
28. J. D. FERRY "Viscoelastic properties of polymers" (Wiley, New York, 1970).
29. B. Z. JANG, D. R. UHLMANN and J. B. VANDER SANDE, *Polym. Eng. Sci.* **25** (1985) 98.
30. H. G. OLF and A. PETERLIN, *J. Polym. Sci.* **12** (1974) 2209.
31. A. PETERLIN, *ibid.* **C9** (1965) 61.
32. *Idem, Kolloid Z. Z. Polym.* **233** (1968) 857.
33. N. ALBEROLA and J. PEREZ, *J. Mater. Sci.* **26** (1991) 2921.
34. G. SHI, *Makromol. Chem.* **190** (1989) 907.
35. R. F. SARAF and R. PORTER, *Polym. Eng. Sci.* **28** (1989) 842.
36. T. LIU and I. R. HARRISON, *Polymer* **28** (1987) 1860.
37. A. MARQUEZ-LUCERO, C. G'SELL and K. W. NEALE, *ibid.* **30** (1989) 636.
38. A. PETERLIN, *J. Mater. Sci.* **6** (1971) 490.
39. N. ALBERORA, M. FUGIER, D. PETIT and B. FILLON, *J. Mater. Sci.* **30** (1995) 0000.
40. I. M. WARD, "Mechanical properties of solid polymers", 2*nd* Edn (Wiley, New York, 1983).

Received 1 March
and accepted 27 July 1994